

5 | Quantitative morphology of nearby field galaxies

R.A. Jansen, M. Franx, D. Fabricant & N. Caldwell, 1997
As submitted for publication in *The Astrophysical Journal*

We describe the morphological properties of galaxies in the local field as a function of passband (U, B & R). The data are part of our photometric and spectrophotometric survey of ~ 200 nearby galaxies selected from the CfA redshift survey catalog. Following Abraham *et al.* (1994, 1996ab), we measure the central concentration and asymmetry of the galaxy images. We find that the image asymmetries of galaxies in our sample depend on the wavelength of observation. The difference between the asymmetry measured in the *U* and *R* bands is correlated with Hubble type and galaxy color, in the sense that the difference is larger for later type galaxies with bluer colors. The dependence of asymmetry on the wavelength of observation suggests that caution is necessary when comparing single wavelength band images of galaxies at a variety of redshifts. We estimate the importance of this effect when comparing galaxy asymmetry in the HST Medium Deep and Hubble Deep Field Surveys.

WE describe the morphologies of a sample of 198 nearby ($z < 0.08$) field galaxies using a simple but quantitative technique developed by Abraham *et al.* (1994, 1996a,b) (hereafter A94, A96a and A96b) for high redshift galaxies in the Hubble Deep Field (HDF). The image of each galaxy is reduced to two parameters: central concentration and asymmetry. Our purpose is to identify the main issues that will affect studies of galaxy evolution, so we explore the dependence of the morphological parameters on limiting isophote and wavelength of observation as well as the more expected correlations with Hubble type and color. Our sample was drawn from the (B-selected) CfA redshift survey to approximately reproduce the observed galaxy luminosity function to $M_B \sim -15$, but without bias as to morphological type.

In section 5.1 we describe the selection details for our sample, the observations and the reduction procedures. In section 5.2 we present the morphological results and their dependence on various parameters. In section 5.3 we discuss the implications of our results if asymmetry is used to search for galaxy evolution.

5.1 Technical Details

5.1.1 Sample selection

Here we report the first results from our photometric and spectroscopic survey of 198 nearby galaxies. Our goal in selecting these galaxies was to obtain an unbiased sample of the galaxy population in the nearby universe that is deep enough to include the dimmer remnants of galaxies that may have been formerly much brighter. Even when we restrict our attention to the local properties of galaxies, a deep sample is necessary because many galaxy properties like color, star formation rate and emission line strength correlate with luminosity (*e.g.*, Moody & Kirshner 1988). We selected galaxies from the first CfA redshift catalogue, which contains galaxies to a limiting blue photographic magnitude (from the Zwicky catalog) $m_Z = 14.5$ (Huchra *et al.* 1983).

For some of our survey goals (discussed elsewhere) we required integrated spectra. Because the FAST spectrograph used to obtain the integrated galaxy spectra has a maximum slit length of $3'$, we wished to minimize the number of

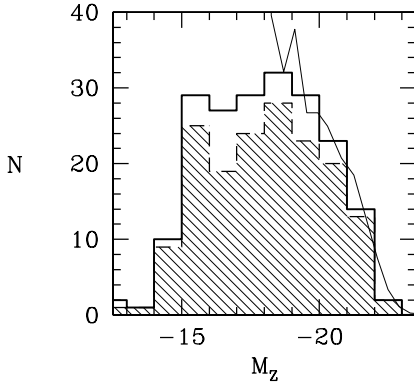


FIGURE 5.1— Histogram of the number distribution of absolute magnitude M_Z in the original sample of 198 galaxies (open histogram) and in the subsample of 165 galaxies used in this paper (hashed). Note the wide range in luminosity sampled by this survey. Marzke *et al.*'s (1994) luminosity function is overplotted for reference. Although the luminosity distribution may not follow exactly the local galaxy luminosity function, any correction should be small.

galaxies larger than the slit length. We did not want to impose a strict diameter limit to avoid biasing against low surface brightness galaxies. Instead we required the high luminosity galaxies in the sample (which are generally the largest) to be more distant by imposing a lower limit on radial velocity that increases with luminosity. After applying a correction for the motion of the Milky Way with respect to the local group, this cutoff is $V_{LG}(\text{km s}^{-1}) > 10^{-0.19-0.2 M_Z}$. Following this cutoff, only a few galaxies larger than $3'$ remain.

We take $V_{LG} = V_{helio} + 300 \cos(b)\sin(l)$, where b is the galactic latitude and l is the galactic longitude. This approximates the result of Yahil *et al.* 1977. Here (and below), we calculate galaxy distances directly from V_{LG} , assuming $H_0=100 \text{ km s}^{-1} \text{ Mpc}^{-1}$.

In order to avoid a sampling bias favoring a cluster population we also excluded galaxies in the direction of the Virgo Cluster with $V_{LG} < 2000 \text{ km s}^{-1}$ in the RA and DEC range given by Binggeli *et al.* (1985). A total of 1006 galaxies are left after our radial velocity and Virgo Cluster cuts. Our goal was to reduce this number to ~ 200 galaxies with a distribution in

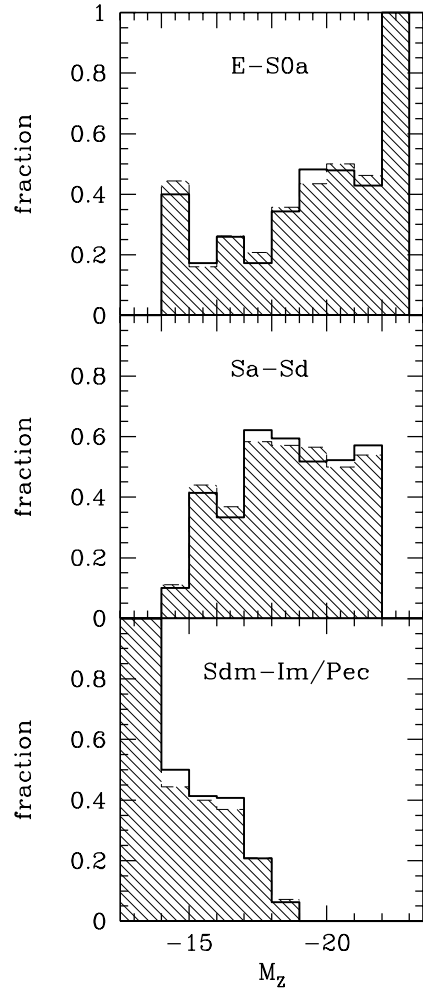


FIGURE 5.2— Fractional distributions for three morphological classes as a function of absolute magnitude. Not surprisingly, at the faint end dwarf irregulars form an important fraction of the sample, at the high end early types. Figures 5.1 and 5.2 show that the 165 galaxies constitute a fair subsample of the original sample in both type and luminosity.

M_Z that approximates the local galaxy luminosity function and that fairly samples the changing mix of morphological types as a function of M_Z . We sorted the sample into 1 magnitude wide bins of M_Z and sorted the galaxies within each bin by morphological type. We selected every N th galaxy in each bin, where N

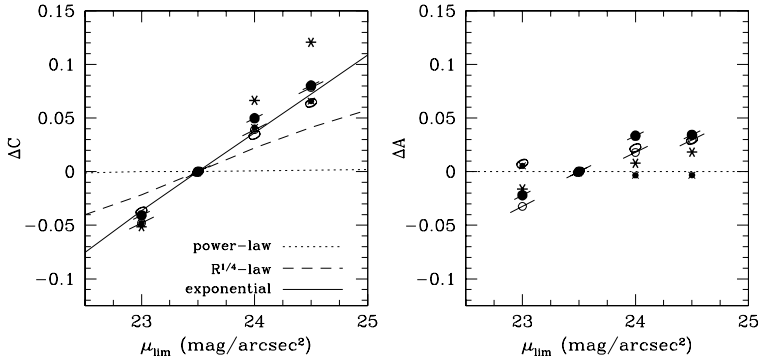


FIGURE 5.3— (a) (left) ΔC (referenced to $23.5 \text{ mag/arcsec}^2$) vs. limiting isophote μ_{lim} . Plot symbols are coded according to morphological type as in figure 5.6. The expected change in the concentration index C for three galaxy models is plotted for reference. Realistic readout- and photon noise were added to the models. Note the strong dependence of C on μ_{lim} in the case of an exponential profile. (b) (right) ΔA vs. limiting isophote.

is the ratio between the total and desired number of galaxies in the bin (determined by the local galaxy luminosity function, *e.g.*, Marzke *et al.* 1994). The morphological types used in the selection were taken from Huchra *et al.* 1983. The types as used in this paper are from a later release of the CfA redshift survey and its extensions (Huchra *et al.* 1997). The main difference between the original and updated types is that the fraction of unclassified spirals has been reduced.

The absolute magnitudes of our sample of 198 galaxies are plotted in Figure 5.1, with the luminosity function of Marzke *et al.* (1994). In what follows, we use data from a subsample of 165 galaxies, and the absolute magnitude distribution of this subsample is also plotted in Figure 5.1 for comparison. The distribution of the morphological types of the original 198 galaxies, as well as the subsample of 165, is shown in Figures 5.2a–c. We conclude that the 165 galaxies are a fair subsample of the original 198 galaxies, and that they can be considered representative of the galaxy population in the local universe.

5.1.2 Observations

The observations reported here were made with CCD cameras at the F. L. Whipple Observatory’s 1.2 m telescope, on Mt. Hopkins, Arizona. The data were obtained during 50 nights between 1994 March and 1997 March. We used both

front-side and back-side illuminated versions of Loral CCDs with 2048×2048 , $15 \mu\text{m}$ pixels. This yields a scale of $\sim 0''.32 \text{ pixel}^{-1}$, although we usually binned the images 2 by 2. The images cover a region $\sim 11'$ square. For both CCDs the readout noise was $\sim 8 e^- \text{ rms}$.

We obtained B and R images with the front-side illuminated CCD, typically integrating $2 \times 900 \text{ s}$ in B and $2 \times 450 \text{ s}$ in R . Beginning in 1995 October, the back-side illuminated CCD camera was commissioned, allowing U exposures. We usually integrated 900 s in U , $2 \times 450 \text{ s}$ in B and $2 \times 180 \text{ s}$ in R with this CCD.

The filters we used closely resemble Johnson (1955) U and B and Cousins (1976) R . On photometric nights, several Landolt (1992) standard star fields were observed, both at low and high airmasses, for photometric calibration. During photometric nights we obtained short exposures to calibrate the non-photometric observations. The resolution of our CCD images was typically between $1''.5$ and $2''.0$ FWHM.

5.1.3 Data Reduction

The data were reduced in the standard manner. After flatfielding with twilight flats, the images are typically flat to better than 0.8% overall, improving to better than 0.5% in the central portion of the CCD normally used for our photometric analysis. The large field of view allowed accurate determination of the sky level for even

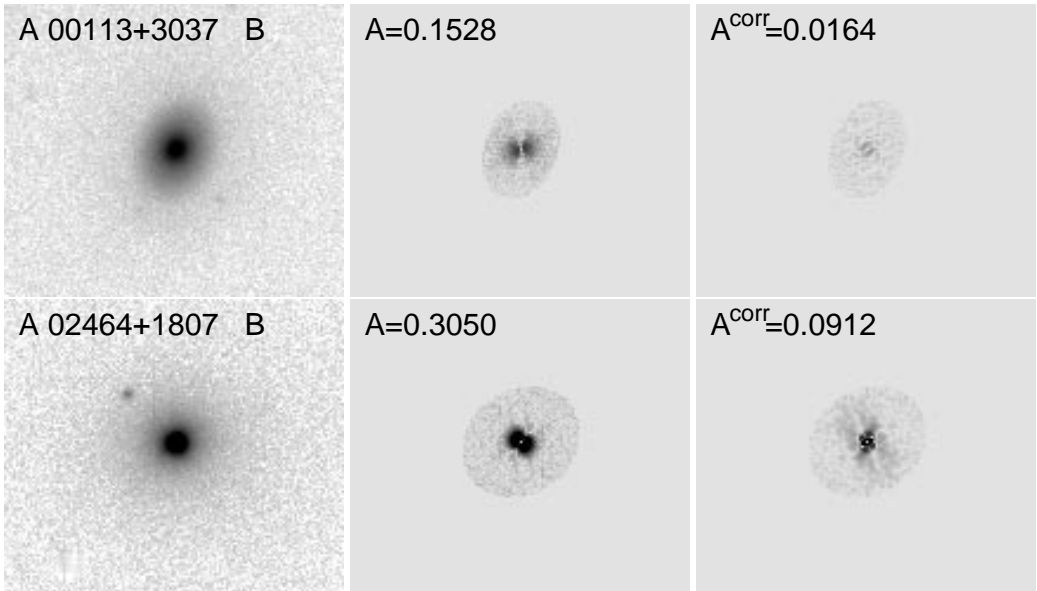


FIGURE 5.4— The effect of pixelation effects on the value of the asymmetry index. Presented are from left to right the greyscale renditions of the B filter image, the original and the corrected rotational difference image for compact ellipticals A00113+3037 (*top*) and A02464+1807 (*bottom*). The double-lobed pattern visible in the middle panels is characteristic for a slight (sub-pixel) mismatch between the center of the light distribution and the center of the brightest pixel.

the largest galaxies in our sample. We fitted ellipses to all galaxy images to obtain radial intensity profiles using the ellipse-fitting procedure described in detail in Franx *et al.* (1989), and references therein. Pixels with CCD defects or cosmic ray events were excluded from the fit. The width of each fitted ellipse was chosen to be 1.1 times that of the previous one. This ensures a nearly constant signal to noise ratio, over a large range in radius.

The radial intensity profiles were photometrically calibrated, solving simultaneously the calibration equations for B and R , or U and R , using $(B-R)$ and $(U-R)$ color terms, respectively. This procedure avoids the introduction of correlated errors in the radial surface brightness profiles due to the two filters used in the color term correction. We measured isophotal magnitudes, half-light radii and colors from the radial surface brightness profiles.

5.1.4 Central concentration and rotational asymmetry

Following A94 we use a quantitative classification system based on the concentration and asymmetry of the galaxian light. For each galaxy we fit an ellipse E with semi-major axis a to the pixels at the specified surface brightness limit after interpolating over the excluded pixels and smoothing with a 3×3 pixel boxcar. All pixels within the ellipse E are used to calculate the morphological parameters, and we interpolate over the excluded pixels within the elliptical aperture.

The concentration index, C , is then defined by:

$$C = \frac{\sum_{E(\alpha)} I_{ij}}{\sum_E I_{ij}}, \quad (5.1)$$

where I_{ij} is the intensity in pixel (i, j) . $E(\alpha)$ is an empirically chosen elliptical aperture with the same ellipticity and orientation as E , but with a smaller semi-major axis, αa (as in Naim *et al.* 1997). We adopt Abraham *et al.*'s choice of $\alpha = 0.3$. C is then the ratio of light within 0.3

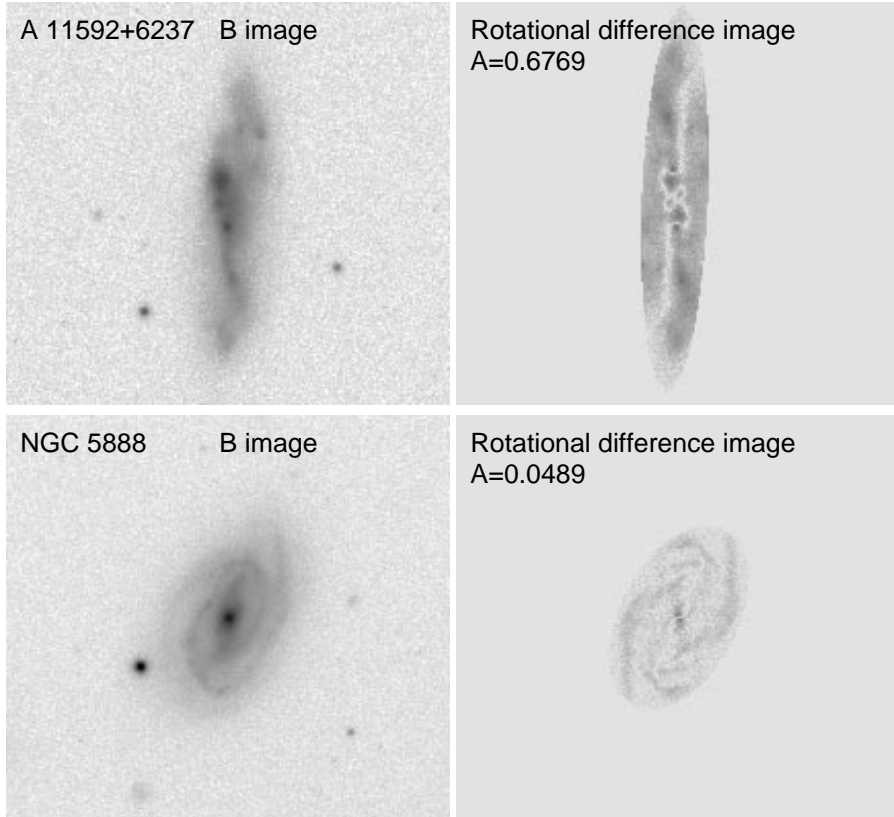


FIGURE 5.5— Greyscale renditions of the B filter image and corresponding rotational difference image for (top) a very asymmetric galaxy, A11592+5237, and (bottom) a very symmetric galaxy, NGC5888. The value of the measured asymmetry index A is indicated. As can be seen for NGC5888, a symmetric image does not need to be featureless.

times the isophotal radius to the light within the isophotal radius.

Again following Abraham *et al.* (A96a), an asymmetry index A is defined by rotating the galaxy image by 180° about its center and subtracting the rotated from the original image, using the aperture E as a mask:

$$A = \frac{1}{2} \frac{\sum_E |I_{ij} - I_{ij}^R|}{\sum_E I_{ij}} - k, \quad (5.2)$$

where I_{ij}^R is the intensity in pixel (i, j) following rotation. The term k is a small correction to account for the contribution of noise in the sky background to A . We determine k by measuring the asymmetry for a region of sky in an

equivalent aperture. We do not correct for the shot noise contribution to A , which we estimate contributes a term of ~ 0.01 to A .

We begin our analysis by measuring asymmetry and concentration indices A and C for the B filter galaxy images with photometric calibration and that reached to at least $\mu_{lim}^B = 23.5$ at 1σ above the sky level. For this analysis we did not attempt to combine multiple images to improve the signal to noise (see exception below) but we averaged the results from those multiple exposures that reached to $\mu_{lim}^B = 23.5$. We then measured the corresponding R and U filter images using the elliptical apertures determined from the B images. We included only the R and U images where the signal level at the boundary

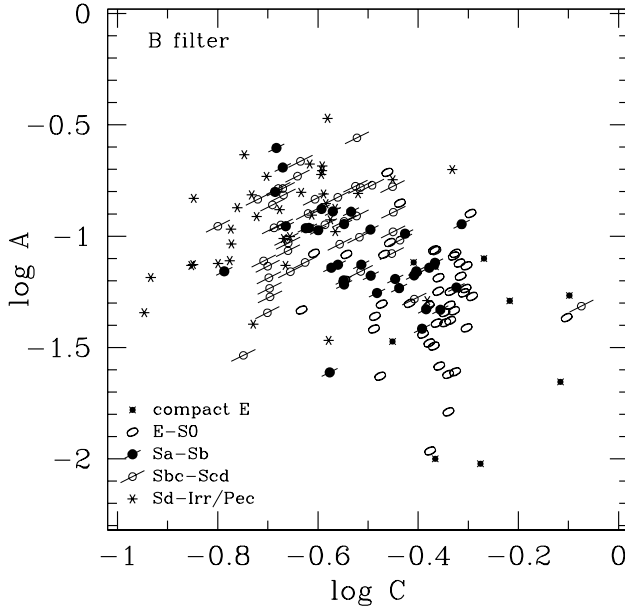


FIGURE 5.6— Distribution of the 165 measured nearby field galaxies in the asymmetry versus central concentration ($\log A$ vs. $\log C$) plane as measured in the B filter. The plot symbols are coded according to morphological type. Small negative values of $\log C$ correspond to high concentration, of $\log A$ to high asymmetry. The early-type galaxies tend to have higher central concentrations and lower asymmetries than the late type galaxies. However, the scatter in both A and C is large for any given morphological type.

of the B aperture is at least 1σ above the sky. The images for 162 of our 198 sample galaxies met these criteria.

We checked to see if the subsample of 162 galaxies is biased against low surface brightness galaxies in the original sample of 198, and found that it is not, except for galaxies with central surface brightnesses $\mu_B \lesssim 22.5$. We removed this bias by combining the two separate B and R images for three low surface brightness galaxies to attain adequate depth, bringing the final sample size to 165 galaxies. In any case, only a small central portion of these galaxies is brighter than $\mu_{lim}^B = 23.5$.

The central concentration parameter, C , depends on the isophote limit chosen (A96a and A96b), unless the galaxy has a surface brightness profile that has a power law dependence on the projected radius. Figure 5.3a illustrates the expected dependence of C on the isophotal limit from model calculations and the measured dependence for galaxies in our sample. The

asymmetry parameter, A , depends on the limiting isophote as well (A96a) because additional structures are included as a is increased. Balancing this however, is the fact that the contributions of these additional features are weighted by their (lower) brightness (Naim *et al.* 1997). Figure 5.3b shows the dependence of A on limiting isophote for our sample. Clearly, standardizing the limiting isophote is required if a comparison between samples is attempted. We adopt $\mu_{lim}^B = 23.5$ in what follows.

5.1.5 Discrete Sampling Effects

The images of most of the galaxies in our sample typically cover several thousand pixels and discrete sampling effects do not affect our measurements of asymmetry. In a few cases, however, the gradient of surface brightness is high, and limited sampling can cause errors in asymmetry measurements if corrective action is not taken. This is a concern for some of the compact ellipticals and galaxies with active nuclei

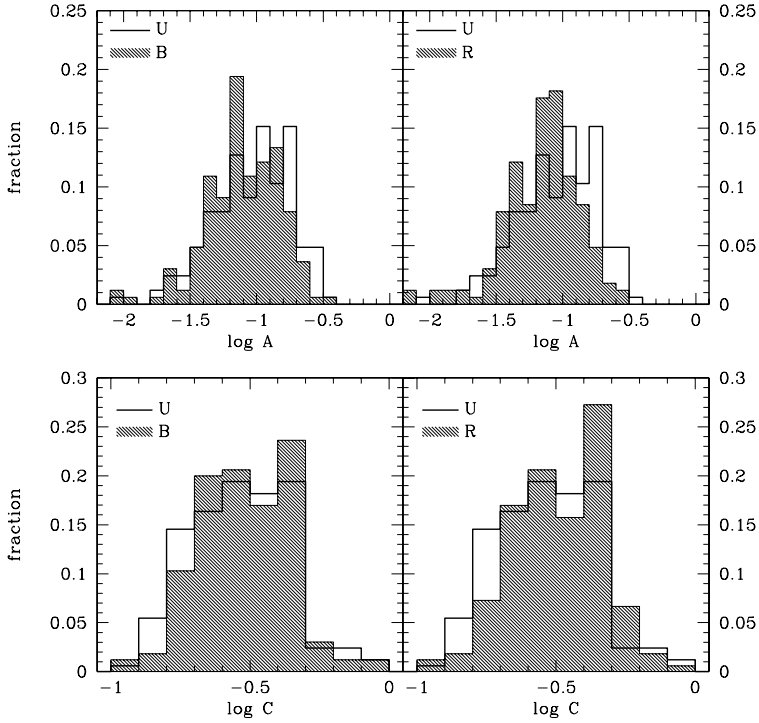


FIGURE 5.7— (top) Comparison of histograms of $\log A$ for (a) U and B filter and (b) U and R filter measurements, respectively. Note the progressive shift towards higher asymmetries going to a bluer passband. (bottom) (c) and (d) Same for $\log C$. The histograms do not differ significantly, although there is a hint of a shift towards higher concentrations for measurements in a redder passband.

in our sample. To illustrate this point we reproduce in Figure 5.4 the B filter greyscale images of two compact ellipticals, A00113+3037 and A02464+1807 (left panels), as well as the rotational asymmetry images derived making no correction for sampling errors (middle panels). A significant signal is present in the difference images, displaying the two-lobed pattern characteristic of a small (sub-pixel) offset between the center of the light distribution and the center of the brightest pixel. The corresponding asymmetry indices are high.

Fortunately, this effect may be simply corrected by rebinning the galaxy images to center the peak of the galaxy surface brightness on a pixel before calculating the asymmetry. When this correction is made, we see a large drop in the signal in the difference image and hence in the asymmetry index (right panels). We found

it necessary to rebin the images of 10 galaxies to avoid sampling errors. This type of sampling error may also be important for coarsely sampled HST data (Abraham, private communication).

5.2 Results

In figure 5.5 we present greyscale renditions of the B filter image and the corresponding rotational difference image for a very asymmetric galaxy, A11592+5237 (Im), and a relatively symmetric one, NGC5888 (SBb). In Figure 5.6 we plot the distribution of the galaxies in the $\log A$ - $\log C$ plane for the B data. The points are coded according to morphological type. The early-type galaxies tend to have higher central concentrations and lower asymmetries than the late type galaxies. However, the scatter in both A and C is large for any given morphological type.

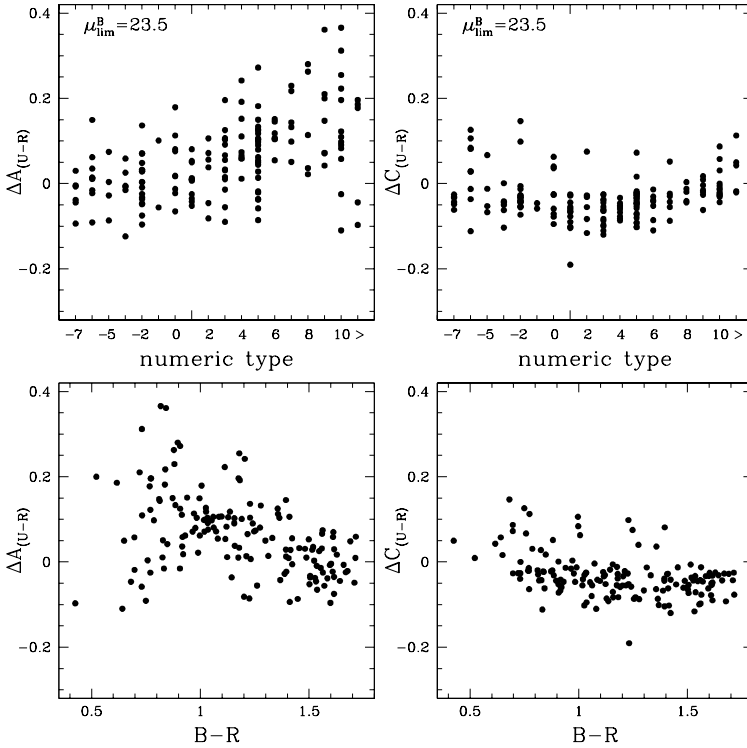


FIGURE 5.8— (a) $\Delta A_{(U-R)}$ as a function of numeric type. Most of the shift in asymmetry seen in figure 5.7 is due to galaxies with types later than Sbc ($t > 4$). (b) Same for $\Delta C_{(U-R)}$. Note the strong correlation with type for types later than S0 ($t > 0$). (c) $\Delta A_{(U-R)}$ as a function of $B-R$ color. The galaxies responsible for the shift in asymmetry tend to be fairly blue. (d) Same for $\Delta C_{(U-R)}$.

In Figure 5.7 we plot the distributions of A and C for the U , B and R images. The asymmetry clearly depends on wavelength in the sense that galaxies tend to be more asymmetric in bluer passbands.

The median (mean) values for $\log A$ are $-0.99(-1.04)$, $-1.11(-1.10)$, and $-1.13(-1.16)$ in U , B and R , respectively. Using a Kolmogorov-Smirnov (K-S) two-sample one-tailed test, we reject the hypothesis that the distributions for U and R are drawn from the same population at the 99.99% significance level (3.7σ). The result for either U vs. B or B vs. R is less convincing ($93.2\%/1.5\sigma$ and $86.6\%/1.1\sigma$ significance, respectively). The central concentration, C , does not depend significantly on the observed wavelength in our sample.

We define $\Delta A_{(U-R)}$ as the difference in A mea-

sured in the U and the R bands. Figure 5.8a shows that this dependence of A on wavelength is due to galaxies of type Sbc and later ($t \gtrsim 4$); for earlier types A varies only weakly with the passband. The dependence of $\Delta A_{(U-R)}$ on type is due to the irregular distribution of starformation regions (where most of the blue and UV light is emitted) within late type galaxies. $\Delta A_{(U-R)}$ progressively increases towards later morphological types. With a Spearman rank correlation test we find that the significance of this correlation is at least 99.99% (6.5σ). Figure 5.8c shows that the galaxies responsible for the dependence of A on wavelength have blue $B-R$ colors. This is not surprising because late-type galaxies have bluer colors than early types.

A similar test for a correlation of $\Delta C_{(U-R)}$ with type (figure 5.8b) gives a marginal result when

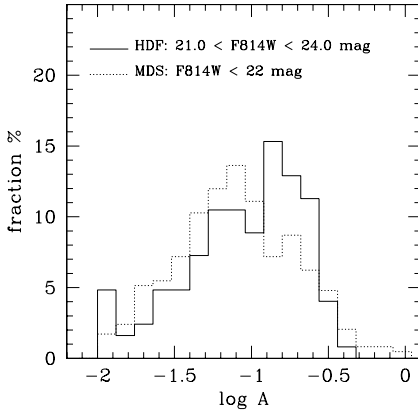


FIGURE 5.9— Histograms of $\log A$ for the HDF and MDS overplotted (reproduced from figure 2 of Abraham *et al.* 1996a). The median values of $\log A$ are -1.06 for the MDS and -0.89 for the HDF.

we include all types (93.7% significance, 1.9σ). If we consider only types later than S_0 , however, there is a clear relation (99.99% significance, 6.2σ).

5.3 Discussion

The fact that the measured asymmetry of the galaxy light depends on the passband for late-type galaxies is important if we try to compare the images of galaxies at a wide range of redshifts in a single passband. One such comparison has been made for the Hubble Space Telescope F814W band observations of galaxies from the Medium Deep Survey (MDS) and the Hubble Deep Field (HDF) (A96a, A96b, van den Bergh 1996). Abraham *et al.* (A96a) find a significant shift in A for two sets of observations with magnitude ranges $F814W < 22$ for the MDS and $21 < F814W < 24$ for the HDF. The shift in the median $\log A$ is ~ 0.17 in the sense that the galaxy images in the HDF are more asymmetric. In Figure 5.9, we replot the data from Figure 2 of A96a. As Ellis (1997) notes, this comparison does not correct for biases due to the changing rest-frame bandpass.

Although a detailed calculation of the differences in asymmetry for the MDS and the HDF that would be predicted from our measurements requires data that we do not have, we

can estimate whether or not the differences in A as a function of passband that we observe at low redshift are likely to affect the comparison of the MDS and HDF galaxies. We must first estimate the median redshifts of the two samples.

A large sample of redshifts for the MDS galaxies are not available. We therefore attempt to estimate the MDS depth from a ground-based I -selected survey. For the 483 galaxies with $I_{AB} \leq 22.0$ in the Canada-France Redshift Survey (CFRS; Lilly *et al.* 1995a,b, Le Fèvre *et al.* 1995, Hammer *et al.* 1995) we calculate a median redshift of 0.51. A K -selected sample of galaxies with $K < 22$ in the HDF (Cowie *et al.* 1996, Cowie 1997) yields a median redshift of ~ 1.0 (using either spectroscopic redshifts or six filter photometric redshifts) if we select the galaxies with $21 < F814W < 24$.

Based purely on the observed shift in A in our sample going from U to R and on the translation of the observed F814W band to the rest frame for the estimated median redshifts of the MDS and the HDF, we would expect a difference in $\log A$ of ~ 0.06 . We therefore can account for only a third of the observed shift in asymmetry between the MDS and HDF surveys. Note, however, that the amplitude of the observed shift depends on the color distribution (see figure 5.8). In the estimate above we assume similar rest-frame color distributions at $z=0$, 0.51 and 1.0.

Acknowledgements

R. A. J. thanks the Harvard-Smithsonian Center for Astrophysics and the F. L. Whipple Observatory for hospitality during several visits, when all of the observations and part of this work was done. This work was partly supported by grants from the Netherlands Organisation for Scientific Research (NWO), the Leiden Kerkhoven-Bosscha Fund, and by the Smithsonian Institution.

References

- Abraham, R. G., Valdes, F., Yee, H. K. C., & van den Bergh, S. 1994, *ApJ*, 432, 75 (A94)
- Abraham, R. G., Tanvir, N. R., Santiago, B. X., Ellis, R. S., Glazebrook, K., & van den Bergh, S. 1996a, *MNRAS*, 279, L47 (A96a)

- Abraham, R. G., van den Bergh, S., Glazebrook, K., Ellis, R. S., Santiago, B. X., Surma, P., & Griffiths, R. E. 1996b, *ApJS*, 107, 1 (A96b)
- van den Bergh, S., Abraham, R. G., Ellis, R. S., Tanvir, N. R., Santiago, B. X., & Glazebrook, K., 1996, *AJ*, 112, 359
- Binggeli, B., Sandage, A., & Tammann, G. A. 1985, *AJ*, 90, 1759
- Cousins, A. W. J. 1976, *MmRAS*, 81, 25
- Cowie, L. L., Songaila, A., Hu, E. M., & Cohen, J. G. 1996, *AJ*, 112, 839
- Cowie, L. L. 1997, http://www.ifa.hawaii.edu/~cowie/k_table.html
- Crampton, D., Le Fèvre, O., Lilly, S. J., & Hammer, F. 1995, *ApJ*, 455, 96
- Ellis, R. S. 1997, *ARA&A*, 35, 389
- Le Fèvre, O., Crampton, D., Lilly, S. J., Hammer, F., & Tresse, L. 1995, *ApJ*, 455, 60
- Franx, M., Illingworth, G., & Heckman, T. 1989, *AJ*, 98, 538
- Hammer, F., Crampton, D., Le Fèvre, O., & Lilly, S. J. 1995, *ApJ*, 455, 88
- Huchra, J. P., Davis, M., Latham, D., & Tonry, J. 1983, *ApJS*, 52, 89
- Huchra, J. P., Geller, M. J., Clemens, C. M., Tokarz, S. R., & Michel A. 1992, *Bull.C.D.S.*, 41, 31 (*CfA Redshift Catalogue*)
- 1997, (*CfA Redshift Catalogue, version Feb 14 1997*)
- Johnson, H. L. 1955, *Ann. Astrophys.*, 18, 292
- Landolt, A. U. 1992, *AJ*, 104, 340
- Lilly, S. J., Le Fèvre, O., Crampton, D., Hammer, F., & Tresse, L. 1995a, *ApJ*, 455, 50 (CFRS)
- Lilly, S. J., Hammer, F., Le Fèvre, O., & Crampton, D. 1995b, *ApJ*, 455, 75
- Lilly, S. J., Tresse, L., Hammer, F., Crampton, D., & Le Fèvre, O. 1995c, *ApJ*, 455, 108
- Marzke, R. O., Huchra, J. P., & Geller, M. J. 1994, *ApJ*, 428, 43
- Moody, J. W., & Kirshner, R. P. 1988, *AJ*, 95, 1629
- Naim, A., Ratnatunga, K. U., & Griffiths, R. E. 1997, *ApJ*, 476, 510
- Yahil, A., Tammann, G. A., & Sandage, A. 1977, *ApJ*, 217, 903
- Zwicky, F., Herzog, E., Wild, P., Karpowicz, M., & Kowal, C. 1961–1968, *Catalogue of Galaxies and of Clusters of Galaxies*, 6 vols., (Pasadena: California Institute of Technology)

